# Sensitivity of uplift patterns to dip of the San Andreas fault in the Coachella Valley, California

**Laura A. Fattaruso[1], Michele L. Cooke[1], and Rebecca J. Dorsey[2]**
[1]*Department of Geosciences, University of Massachusetts, Amherst, Massachusetts 01003, USA*
[2]*Department of Geological Sciences, University of Oregon, Eugene, Oregon 97403, USA*

## ABSTRACT

**Three-dimensional mechanical simulations of the San Andreas fault system within the Coachella Valley in southern California produce deformation that matches geologic observations and demonstrate the first-order impact of fault geometry on uplift patterns. To date, most models that include the Coachella Valley segment of the San Andreas fault have assumed a vertical orientation for this fault, but recent studies of seismicity and geodetically observed strain suggest that this segment of the fault may dip 60°–70° to the northeast. We compare models with varied geometry along this segment of the fault and evaluate how well they reproduce observed uplift patterns in the Mecca Hills and Coachella Valley. Incorporating well-constrained fault geometry in regional models will provide a more accurate understanding of active faulting in southern California, which is critical for rupture and hazard modeling that is used to identify regions most susceptible to earthquake damage.**

**We have tested three boundary-element method models for the active geometry of the Coachella Valley segment of the San Andreas fault: one contains a vertical Coachella segment, the second contains a northeast ~65° dipping Coachella segment, and the final alternative contains a vertical Coachella segment plus a subparallel northeast-dipping fault at depth. This final model honors the geometric interpretation of seismicity from the Southern California Earthquake Center Community Fault Model version 4.0. The models containing vertical Coachella Valley segments both produce uplift between the San Andreas and San Jacinto faults that is more uniformly distributed than geologic observations suggest, and these models fail to produce uplift in the Mecca Hills. The dipping model produces tilting of the Coachella Valley consistent with geologic observations of tilting between the San Jacinto and San Andreas faults. The dipping model also produces relative subsidence southwest of the fault and localized uplift in the Mecca Hills that better match the geologic observations. These results suggest that the active Coachella Valley segment of the San Andreas fault dips 60°–70° to the northeast.**

## INTRODUCTION

Vertical crustal motion is a widely observed aspect of deformation in regions of continental strike-slip tectonics such as along the San Andreas fault in California (e.g., Sylvester and Smith, 1976; Rymer, 1991; Roeske et al., 2007; Spotila et al., 2007). Previous mechanical modeling has demonstrated that complex fault geometry exerts a primary control on deformation (e.g., Marshall et al., 2008; Meigs et al., 2008). In southern California, plate interactions and fault structure are complex (Fig. 1)—with a reduction of strike-slip rates along the San Andreas fault through the San Gorgonio Pass (Herbert and Cooke, 2012; McGill et al., 2012) and a transfer of deformation east of the San Andreas fault into the eastern California shear zone (Oskin et al., 2007). Plate motion is also taken up on strike-slip faults subparallel to and west of the San Andreas fault, including the San Jacinto fault and Elsinore fault. This region is well suited for investigating the mechanisms by which fault geometry controls vertical deformation, as recent studies have provided new interpretations of the subsurface fault geometry and improved understanding of active vertical deformation (e.g., Lin et al., 2007; Fuis et al., 2012; Lin, 2013; Lindsey and Fialko, 2013). Mechanical models that simulate vertical deformation can also provide insight into the effects of different active fault geometries on off-fault deformation patterns.

To date, most models investigating deformation, stress, rupture, and ground shaking have assumed that the southern San Andreas fault is vertical (e.g., Carena et al., 2004; Becker et al., 2005; Meade and Hager, 2005; Smith-Konter and Sandwell, 2009; Spinler et al., 2010; Loveless and Meade, 2011; Herbert and Cooke, 2012; Luo and Liu, 2012). However, seismicity, seismic imaging, aeromagnetic data, and recent strain observations from global positioning system (GPS) and interferometric synthetic aperture radar (InSAR) suggest that the active Coachella segment of the San Andreas fault dips 60°–70° NE (Lin et al., 2007; Fuis et al., 2012; Bauer et al., 2013; Fuis et al., 2013; Lin, 2013; Lindsey and Fialko, 2013). An alternative fault geometry that accounts for the pattern of microseismicity described by Lin et al. (2007) has been included in the latest version of the Southern California Earthquake Center (SCEC) Community Fault Model (CFM) version 4.0 (Nicholson et al., 2012). In this interpretation, it is assumed that seismicity occurs along a second fault system that strikes subparallel to the San Andreas fault (Fig. 2). These uncertainties motivate us to explore three alternative possibilities for the geometry of the Coachella segment of the San Andreas fault (Fig. 2). Additionally, we include smaller en echelon faults on the northeast side of the San Andreas fault in the Indio and Mecca Hills (Fig. 3); these faults have not been included in previous mechanical modeling studies (e.g., Cooke and Dair, 2011; Herbert and Cooke, 2012). Geologic and stratigraphic relationships in the Mecca Hills reveal localized uplift and subsidence patterns (e.g., Boley et al., 1994; Sheridan and Weldon, 1994; McNabb, 2013; McNabb et al., 2013) that can be compared to mechanically modeled deformation. We use localized uplift patterns in the Mecca Hills to assess the most plausible geometry for the San Andreas fault in the Coachella Valley and better understand the interplay of fault geometry and deformation.

*Geosphere*; December 2014; v. 10; no. 6; p. 1235–1246; doi:10.1130/GES01050.1; 9 figures; 1 table; 1 supplemental file.
Received 5 March 2014 ♦ Revision received 26 August 2014 ♦ Accepted 28 August 2014 ♦ Published online 12 November 2014

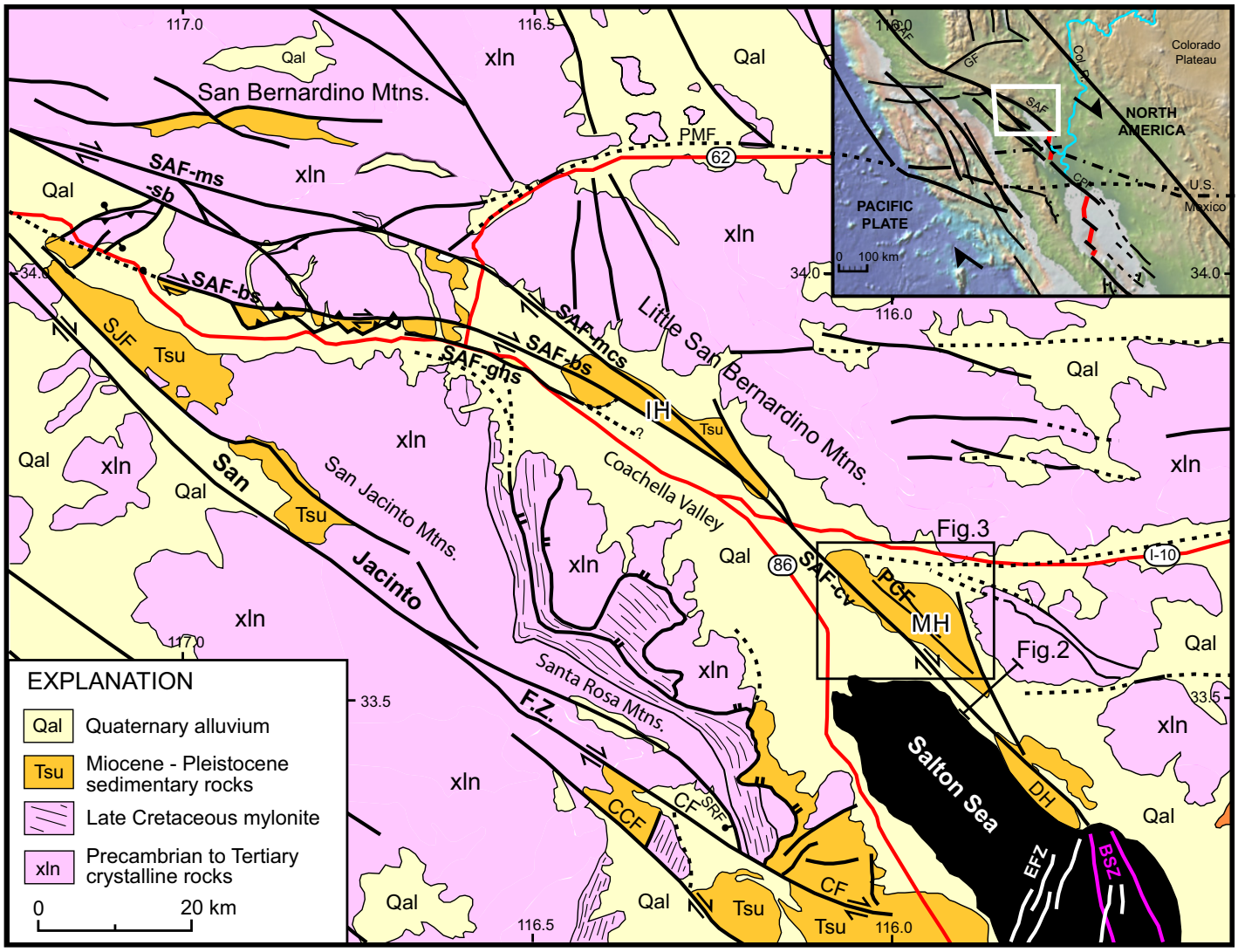


**Figure 1. Simplified geologic map of the Coachella Valley region (compiled from Jennings, 1977; Matti et al., 1992; Powell, 1993; Axen and Fletcher, 1998; Janecke et al., 2010; Weldon, 2011, personal commun.), with faults shown in black and highways in red. Inset shows location within southwestern North America. Abbreviations: BSZ—Brawley seismic zone; CCF—Coyote Creek fault; CF—Clark fault; CPF—Cerro Prieto fault; DH—Durmid Hill; EFZ—Extra fault zone; GF—Garlock fault; IH—Indio Hills; MH—Mecca Hills; PCF—Painted Canyon fault; PMF—Pinto Mountain fault; SAF—San Andreas fault: -bs—Banning strand; -cv—Coachella Valley segment; -ghs—Garnet Hill strand; -ms—Mill Creek strand; -mcs—Mission Creek strand; -sb—San Bernardino segment; SJF—San Jacinto fault; SRF—Santa Rosa fault.**

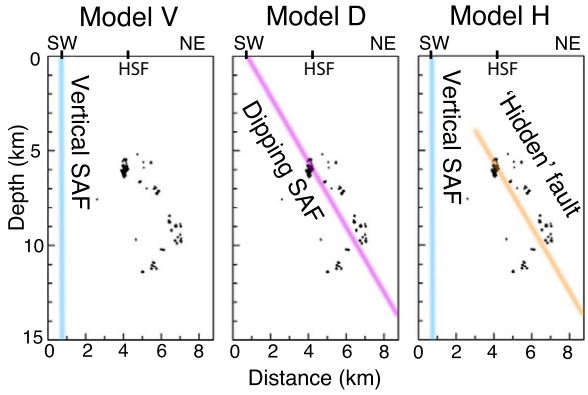


**Figure 2. Three models for the geometry of the Coachella Valley segment of the San Andreas fault (SAF) used in this study. Line of NE-SW cross section is shown in Figure 1. Black dots are seismicity cross sections from Lin et al. (2007). Black dashes at surface represent the location of the surface traces of San Andreas fault and Hidden Springs fault (HSF).**

Our model results show that a northeast dip to the Coachella Valley segment of the San Andreas fault better matches the geologic data of vertical motion than a model with a vertical San Andreas fault. The geometry of the Coachella Valley segment of the San Andreas fault may have significant implications for ground shaking from an earthquake rupture through this region. Dynamic simulations of rupture on dipping faults show that the hanging walls of such faults endure much greater shaking than footwall regions (e.g., Oglesby et al., 2000; Fuis et al., 2013). Furthermore, this section of the San Andreas fault has a high likeli-

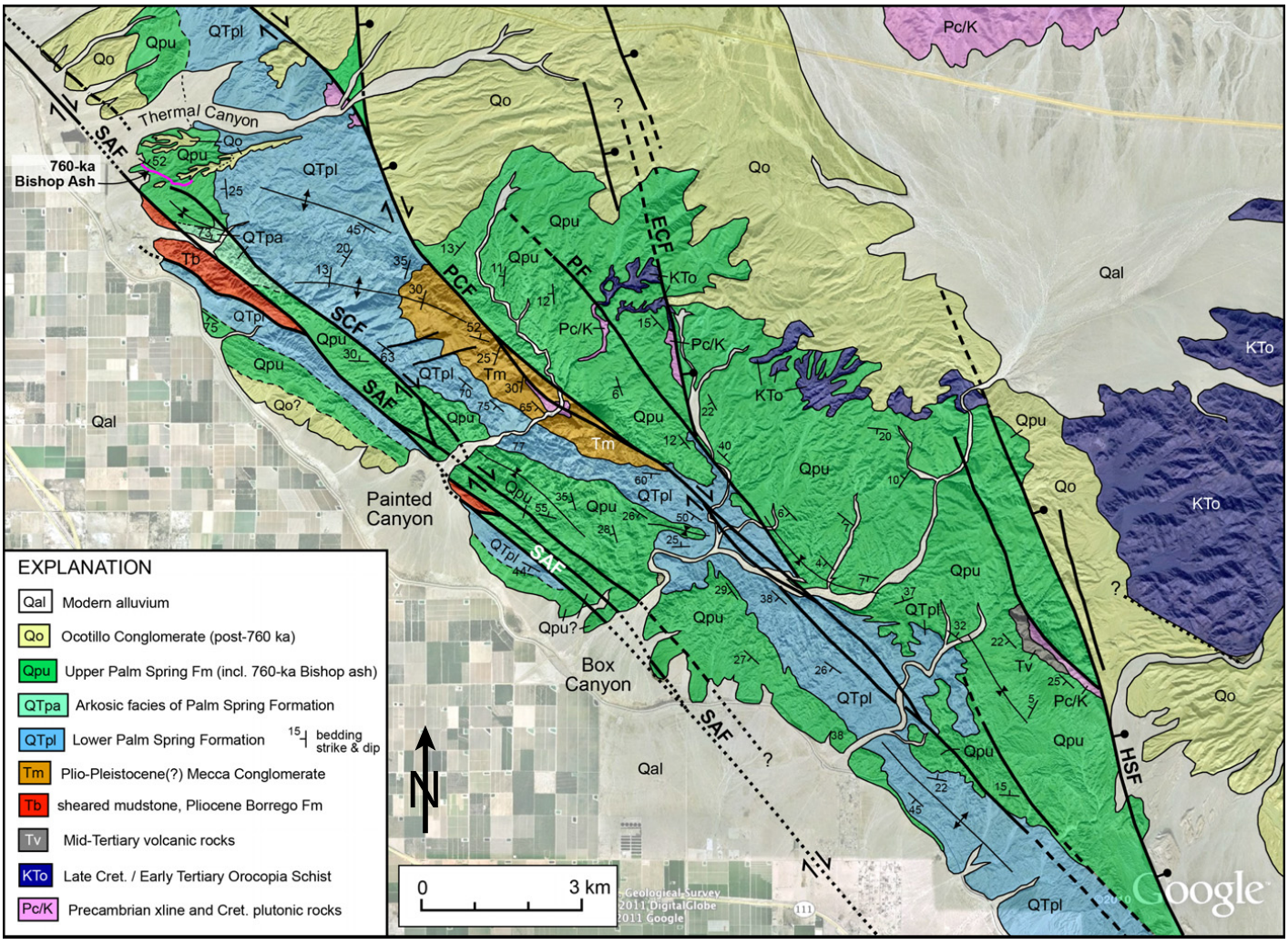


**Figure 3. Geologic map of Mecca Hills (location noted on Fig. 1), compiled from Sylvester and Smith (1976), Rymer (1991, 1994), Weldon (2011, personal commun.), and McNabb (2013). Abbreviations: ECF—Eagle Canyon fault; HSF—Hidden Springs fault; PCF—Painted Canyon fault; PF—Platform fault; SAF—San Andreas fault; SCF—Skeleton Canyon fault.**

hood of rupture in the near future as it has been ~340 years since the last major rupture, and recurrence intervals for such events are bracketed at 116–202 years (Philibosian et al., 2011). In light of this seismic hazard, it is critical that models incorporate accurate fault geometry in order to accurately assess hazard.

## GEOLOGIC BACKGROUND

The San Andreas fault in the Coachella Valley consists of a single main segment along the eastern edge of the valley that splits into the Banning and Mission Creek strands where Interstate 10 crosses the fault (Fig. 1). The fault zone contains many geomorphic features that record recent and ongoing deformation, including dextrally deflected and beheaded streams, shutter ridges, sags, fault scarps, and displaced Quaternary alluvial fans (Keller et al., 1982; Bilham and Williams, 1985; Sieh and Williams, 1997; Rymer, 2000; Shifflett et al., 2002; van der Woerd et al., 2006; Behr et al., 2010). The Late Quaternary strike-slip rate along this segment of the fault is bracketed between 12 and 22 mm/yr, with a preferred rate of 14–17 mm/yr (Behr et al., 2010). During much of the Pleistocene, the San Andreas fault did not occupy the margin of a basin but was embedded in a tectonic lowland with deposition across the active fault trace (Axen and Fletcher, 1998). Pleistocene deposits from formerly subsided parts of the basin were later uplifted within the Mecca Hills within complex folds that illuminate the deformational history (Sylvester and Smith, 1976; Rymer 1991, 1994).

### Structural Interpretation: Is the Coachella Valley Segment of the San Andreas Fault Vertical?

Most deformation models of southern California, including those used for seismic hazard analysis, assume that the active surface of the San Andreas fault is vertical in the Coachella Valley (e.g., Carena et al., 2004; Becker et al., 2005; Meade and Hager, 2005; Smith-Konter and Sandwell, 2009; Spinler et al., 2010; Loveless and Meade, 2011; Herbert and Cooke, 2012; Luo and Liu, 2012). However, a variety of evidence has accumulated in recent years suggesting that the active surface of the San Andreas fault in the Coachella Valley dips between 60° and 70° to the northeast (Fialko, 2006; Lin et al., 2007; Fuis et al., 2012; Lin, 2013; Lindsey and

Fialko, 2013). Fuis et al. (2012) found that a 65° northeast-dipping San Andreas fault produces the best fit to magnetic gradients due to bedrock variations along a transect through the Little San Bernardino Mountains. Because magnetic anomalies from the basement rocks reflect deformation over a long period of time, this record reflects overall cumulative deformation through time, and not necessarily active fault geometry today. Data from recent microseismicity and geodesy also support nonvertical active fault geometry (Fialko, 2006; Lin et al., 2007; Lin, 2013; Lindsey and Fialko, 2013). Seismicity locations from Lin et al. (2007) show clusters of seismicity from 6 to 11 km depth that, when projected vertically to the surface, are offset 3–5 km to the northeast of the surface trace of the San Andreas fault (Fig. 3). The projected locations off the fault trace are well beyond the range of uncertainty in locating methods, which suggests that the active segment of the San Andreas fault in this region dips to the northeast, or, alternatively, occurs on a separate fault located northeast of the San Andreas fault (Nicholson et al., 2012; Nicholson et al., 2013). More recent relocations are consistent with this interpretation (Lin, 2013). Furthermore, geodetic observations from InSAR line-of-sight (LOS) velocities and GPS stations have identified a systematic strain-rate asymmetry across the San Andreas fault in the Coachella Valley (Fialko, 2006; Lindsey and Fialko, 2013). Possible explanations for the asymmetry include nonvertical fault geometry and material heterogeneity across the fault. Lindsey and Fialko (2013) determined that an unrealistically high contrast in material properties across the fault would be needed to explain the observed asymmetry in strain rate, and that models including a 60° northeast dip on the San Andreas fault best match geodetic observations and provide the most feasible explanation for the strain-rate asymmetry.

### Deformation in the Coachella Valley

Recent studies document active northeast tilting of the southern Santa Rosa Mountains and Coachella Valley between the San Andreas and San Jacinto faults (Dorsey et al., 2012). Gravity data reveal northeastward thickening of sediments in the Coachella Valley, suggesting increased subsidence to the northeast (Langenheim et al., 2005; Langenheim et al., 2007). Exposure of Pliocene marine deposits at high elevation in the southern Santa Rosa Mountains requires post-Pliocene uplift of at least ~600 m (Matti et al., 2002). Steep range front morphology, prominent fault facets, large landslides on the faulted western flank of the Santa Rosa Mountains, and the presence of large alluvial fans on the eastern flank record significant asymmetric tilting to the northeast (Dorsey et al., 2012). An abrupt subvertical discontinuity in the thickness of subsurface sediment at the San Andreas fault, from several kilometers on the southwest side to <1 km on the northeast side (Langenheim et al., 2007; Fuis et al., 2012) implies relative subsidence on the southwest side of the Coachella Valley segment of the San Andreas fault.

Transpressional deformation and localized uplift are observed northeast of the San Andreas fault in the Mecca Hills (e.g., Sylvester and Smith, 1976; Rymer, 1991; Rymer, 1994; Sheridan and Weldon, 1994). Nonmarine sedimentary rocks are exposed in a thick section that rests nonconformably on Mesozoic and Precambrian crystalline basement rock (Sylvester and Smith, 1976; Dibblee, 1986, 1997; Boley et al., 1994). The 760-ka Bishop ash and 740-ka Thermal Canyon ash near the top of the section (Rymer, 1989, 1991, 1994) and preliminary new paleomagnetic data (Messe et al., 2012, 2013; McNabb, 2013; McNabb et al., 2013) provide additional constraints on depositional age. Uplift magnitude and rate vary throughout the Mecca Hills, as indicated by variable depth of erosion into sedimentary and basement rocks. The largest magnitude of uplift is observed on the southwest side of the Painted Canyon fault, where Mecca Conglomerate (Pliocene–Pleistocene) on the southwest side is juxtaposed against Upper Palm Spring Formation (mid-late Pleistocene) on the northeast side (Boley et al., 1994; McNabb, 2013; McNabb et al., 2013).

The trace of the San Andreas fault is neither sharply defined nor perfectly linear in this area. In some places its exposure is marked by red clay mélange with heavily strained blocks of sandstone containing Colorado River sediment. A possible source for this mélange may be the Borrego Formation (ca. 2.9–1.2 Ma), which is not mapped in this region but may underlie the exposed sediments (McNabb, 2013). The exposure of the Borrego Formation suggests vertical transport of material up the fault, possibly in conjunction with dip slip, which can be enhanced by nonvertical fault geometry.

## MODEL SETUP

In this paper, we investigate the uplift pattern for three alternative configurations of the San Andreas fault in the Coachella Valley (Fig. 2): vertical San Andreas fault (Model V), northeast-dipping San Andreas fault (Model D), and a combination of both a vertical San Andreas fault and an adjacent northeast-dipping structure based on the SCEC CFM v. 4.0 (Model H). The differences in uplift patterns from these models will reveal the sensitivity of uplift to these variations in fault geometry. Furthermore, the uplift patterns resulting from these models will be compared to the overall tilt of the Coachella Valley as well as the pronounced and localized uplift within the Mecca Hills to constrain the active fault configuration.

We use the three-dimensional boundary-element method (BEM) code Poly3D, which solves the governing differential equations of deformation using continuum mechanics (e.g., Crouch and Starfield, 1990; Thomas, 1993). Fault geometries used in the model (Fig. 4) are based on fault surfaces from the SCEC CFM, which are compiled from geologic mapping, seismicity, and geophysical data (Plesch et al., 2007). Previous refinements to CFM fault geometry that improve match to geologic slip rates along the faults are included in these models (Herbert and Cooke, 2012). The three-dimensional fault surfaces are discretized into triangles of constant slip and zero opening and lie within a linear-elastic and homogeneous material (Fig. 4). The triangular elements of these BEM models are particularly well suited for modeling the complex fault network of southern California because branching and curving fault surfaces with incomplete intersections, such as within the CFM, can be simulated without compromising the accuracy of the results.

Previous Poly3D models have constrained the geometry of active faulting in southern California by comparing the model results to uplift patterns (Meigs et al., 2008; Cooke and Dair, 2011) and fault slip rates (e.g., Marshall et al., 2008; Cooke and Dair, 2011). Boundary-element method investigations of alternative fault configurations (e.g., Griffith and Cooke, 2004; Marshall et al., 2008; Meigs et al., 2008; Dair and Cooke, 2009; Herbert et al., 2014) demonstrate that the three-dimensional fault geometry and connectivity exhibit first-order effects on the distribution of deformation within these fault systems, including uplift patterns (Meigs et al., 2008; Cooke and Dair, 2011). Consequently, changes in fault geometry along the Coachella Valley segment of the San Andreas fault, and the inclusion of secondary faults in Indio and Mecca Hills, may exert a substantial influence on uplift within the region.

Our model of the southern San Andreas fault extends from the Salton Sea past the intersection with the Garlock fault in the north and includes faults of the eastern California shear zone and the San Jacinto fault. The fault geometry follows that used in Herbert and Cooke (2012) with one modification. In addition to exploring a dipping Coachella segment of the San Andreas fault and adding secondary faults within the

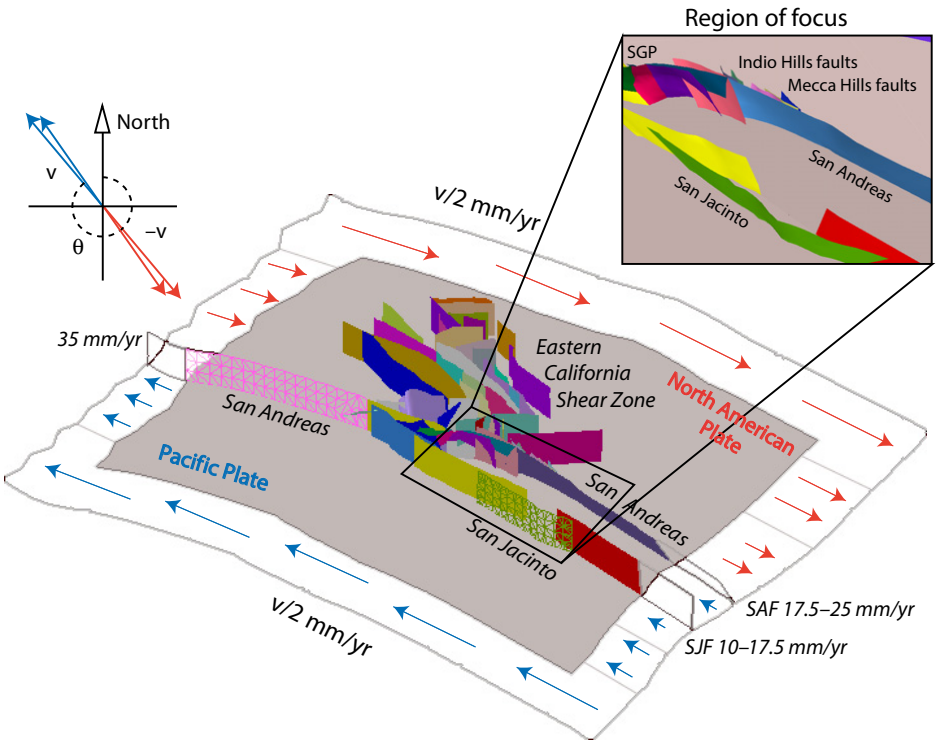


**Figure 4. Oblique view of the model setup and fault surfaces. Faults are discretized into triangular mesh as shown along northern section of San Andreas fault (SAF) and Coyote Creek section of San Jacinto fault (SJF). Half the plate motion (v) is applied to the southwest and northeast edges of the base of the model, at 35 km depth. Applied plate motion decreases stepwise toward the center of the model along the northwest and southeast edges as indicated by arrows. Where faults extend outside the boundary of the model, we prescribe slip rates along edge faults.**

Mecca Hills, we updated the Banning strand of the San Andreas fault to dip ~65°–75° northeast. This modification increased dip-slip rates on the Banning strand by ~2 mm/yr, with corresponding increased uplift northeast of the fault, but it did not have a significant impact on strike-slip rates. This geometry, which subparallels the adjacent Garnet Hill fault, follows the SCEC CFM v. 4.0 (Nicholson et al., 2012).

Fault surfaces are extended to the freely slipping base of the model at 35 km depth, which simulates distributed deformation below the seismogenic crust (Fig. 4). In the crust, seismogenic slip on discrete fault surfaces extends to depths between ~10 and 15 km; but by extending the fault surfaces in the model to 35 km depth, we prevent slip from being artificially constrained at the base of the modeled faults. Faults in the model are frictionless, simulating low frictional slip over multiple earthquake cycles. The results cannot accurately represent deformation on time scales greater than ~100,000 years due to the inelastic processes operating in the crust (e.g., microcracks, calcite twinning, pressure solution, etc.) that are important on longer time scales within folds and are not captured by elastic modeling. Consequently, as with previous models of uplift rate patterns (Meigs et al., 2008), we compare the pattern of uplift rates from these models to the geologic patterns and are not concerned with matching absolute uplift rates.

We apply plate boundary velocities along the base of the models far from the investigated faults so that the interior parts of the model base and all faults are free to slip and interact without prescribed rates of slip (Fig. 4). Subsequently, the faults slip in response to a combination of tectonic loading and interaction with one another. Following Herbert and Cooke (2012), tectonic loading is applied for a range of velocities and orientations constrained by GPS studies and global plate motion models that estimate plate motion of ~45–50 mm/yr at orientations between 320° and 325° (e.g., DeMets et al., 2010). These models do not include any faults west of the San Jacinto fault, which are estimated to accommodate ~5 mm/yr of the plate motion (e.g., Platt and Becker, 2010); so we subtract this rate of motion from the net velocity applied to the models. The modeled slip rates presented in this study are averaged from models with applied tectonic loading at the fastest (45 mm/yr applied at 320°) and slowest (40 mm/yr applied at 325°) rates. Where the San Andreas and San Jacinto faults extend outside the model boundaries, we apply geologic slip rates on edge patches of the faults. This includes a rate of 35 mm/yr applied along the central segment of the San Andreas fault at the northern edge of the models (Weldon and Sieh, 1985). On the southeast edge of the model, slip is partitioned between the San Andreas and San Jacinto faults, but the appropriate partitioning of strike-slip rate between the San Andreas and San Jacinto faults in the Coachella Valley remains a subject of debate. The large range in published strike-slip rates along the San Jacinto fault from 1.9 to >20 mm/yr does not yield sharp constraints on slip-rate partitioning (Sharp, 1981; Prentice et al., 1986; Kendrick et al., 2002; Rockwell, 2008; Janecke et al., 2010; Blisniuk et al., 2011). To incorporate the uncertainty of slip partitioning between the San Andreas and San Jacinto faults, we vary the slip applied at the southern edge of our models, from equal loading of 17.5 mm/yr on both faults, to unequal loading with 10 mm/yr on the San Jacinto fault and 25 mm/yr on the San Andreas fault at the southeast edge of the model. We do not explore a San Jacinto fault > San Andreas fault scenario because there is not significant support for this scenario in the literature.

To investigate the role of San Andreas fault geometry on regional deformation, we test three models for the geometry of the Coachella Valley segment of the San Andreas fault (Fig. 2): Model V incorporates a vertical San Andreas fault; Model D incorporates a northeast-dipping San Andreas fault (see Supplemental File[1]); and Model H incorporates a vertical San Andreas fault with an adjacent, subparallel-dipping fault at depth, as represented in the SCEC CFM v. 4.0 (Nicholson et al., 2012). We have renamed this dipping fault at depth the Hidden fault, from its name in the CFM as the Hidden Springs fault, to avoid confusion with another mapped fault in the region named the Hidden Springs fault. The geometry for the Hidden fault and secondary faults in Indio Hills and Mecca Hills is based on fault geometries from the latest SCEC CFM v. 4.0 (Nicholson et al., 2012). For Model D, the dip of the San Andreas fault varies along strike from 60° to 70°, with an average dip of ~67° to the northeast (see Supplemental File

[1]Supplemental File. 3D PDF of Model D mesh (preferred Model). If you are viewing the PDF of this paper or reading it offline, please visit http://dx.doi.org/10.1130/GES01050.S1 or the full-text article on www.gsapubs.org to view the Supplemental File.

[see footnote 1]). Secondary faults extend from the surface to depths of 3–10 km. These faults merge at depth with the San Andreas fault in Model D and the Hidden fault in Model H. In Model V, the secondary faults do not intersect with the San Andreas fault at depth, and they are consequently unconnected to any larger fault. The subparallel traces of the Painted Canyon fault and Platform fault are within 1 km of one another in some locations and cannot be resolved separately by our mesh. For modeling purposes, a region in which these two faults are within ~1 km has been simplified into a single fault surface, with splays to the north and northeast where the faults diverge.

### Effect of Slip-Rate Partitioning Applied to the Model Boundaries

To explore the impact of slip partitioning between the San Andreas and San Jacinto faults, we applied different slip rates where the faults extend beyond the southern boundary of our models. Herbert and Cooke (2012) found that although changes to the slip rates applied at the edges of the model have some effect on strike-slip rates nearest the model boundaries, changes to model-edge slip rates do not impact matches to the geologic strike-slip rates near the San Gorgonio Pass, which was the focus of that study. We use the same approach as Herbert and Cooke (2012) and incorporate a revised fault configuration for the Coachella Valley to assess the impact of slip partitioning along the southern model boundary on slip rates in the Coachella Valley. The impact of boundary loading for all three fault geometries is similar, and for the sake of brevity, we show the results only for Model D, which we later show to be our preferred model. We compare strike-slip rates for models with loading at the southern edge of the model equally split between the San Andreas and San Jacinto faults (17.5 mm/yr on both) and with greater strike-slip rates applied on the San Andreas fault relative to the San Jacinto fault (25 mm/yr on San Andreas fault; 10 mm/yr on San Jacinto fault; Fig. 5). As expected, equal loading on the southern edges of the faults produces a greater strike-slip rate on the San Jacinto fault and lower strike-slip rate on the San Andreas fault relative to unequal loading. Interestingly, the shapes of the slip-rate curves do not change significantly (Fig. 5). The maximum increase in strike-slip rate along the San Jacinto fault within this region of ~1 mm/yr (Fig. 5) is far less than the 7.5 mm/yr strike-slip rate increase along the southern edge of the model, while the maximum decrease in strike-slip rates along the San Andreas fault (2 mm/yr) is less than the 7.5 mm/yr decrease in boundary loading. The lack of proportionate changes in strike-slip rates with these changes to the applied loading demonstrates that fault geometry exerts a large control on the distribution of strike-slip rates. Fault strands farther from the edge of the model are affected less by the change in boundary loading than faults near the southern boundary.

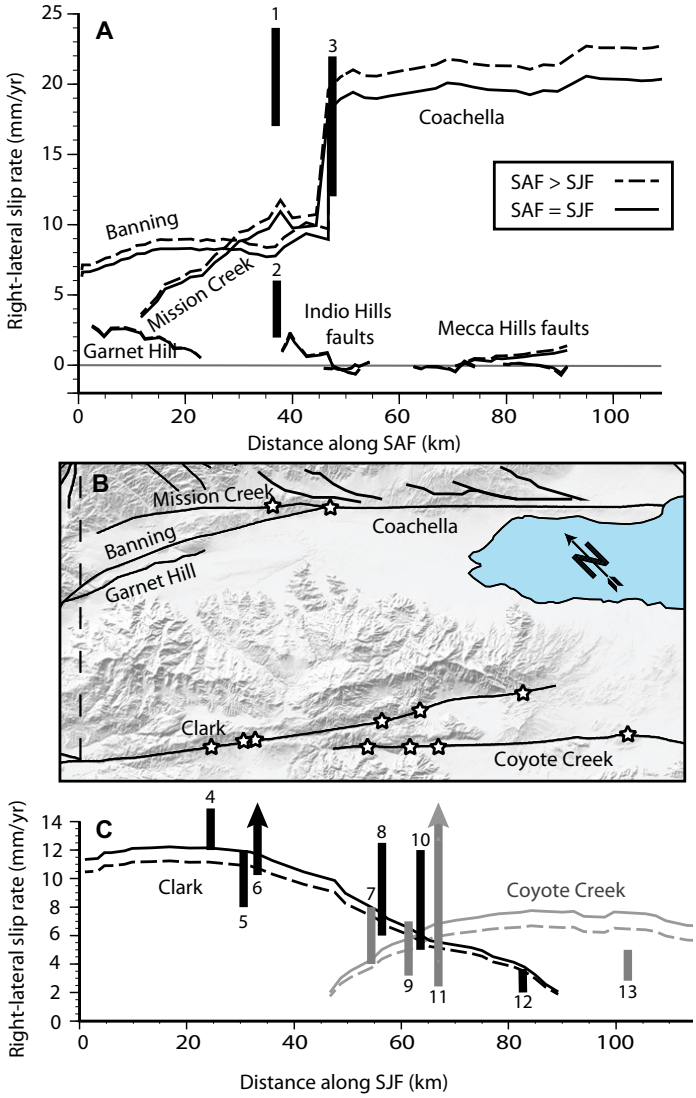


**Figure 5. Strike-slip rate profile (NW to SE) from Model D for (A) the San Andreas fault (SAF) and nearby faults, with (B) mapped fault traces for reference. (C) Strike-slip profile for the San Jacinto fault (SJF). Figures compare models with different loading on edge cracks at the southern edge of the model. Dashed lines represent results from models with 25 mm/yr applied to the SAF and 10 mm/yr to the SJF at the edge of the model; solid lines represent results from models with 17.5 mm/yr applied to both the SAF and SJF. Vertical bars represent geologic strike-slip rates, color coded by strand for the different sections of the SJF. 1—Blisniuk et al., 2012; 2—Fumal et al., 2002; 3—Behr et al., 2010; 4—Rockwell, 2008; 5 and 13—Sharp, 1981; 6, 7, 8, 9, 10, and 12—Blisniuk et al., 2011; 11—Janecke et al., 2010.**

The wide range of published geologic strike-slip rates for the San Jacinto fault does not provide a narrow enough constraint to prefer one loading scenario over the other. The variations between observed slip rates likely reflect spatial variation in slip rates due to interaction among the fault segments (Blisniuk et al., 2011). The

small changes in dip-slip rates along the faults in the model under different boundary loading (Table 1) yield associated minor changes in uplift rates. For the sake of simplicity, and because the resulting changes are small, the model results presented in this paper are from models with equal strike-slip loading rates on the southern edges of the San Jacinto and San Andreas faults.

## COMPARISON OF UPLIFT AND SLIP RATES TO GEOLOGIC RECORD

### Sensitivity of Strike-Slip Rates to Fault Configuration

Comparison of the strike-slip rates produced by the three different structural models to available geologic rates along the faults (e.g., Dair and Cooke, 2009; Herbert and Cooke, 2012) reveals that strike-slip rates do not vary significantly with these changes to fault geometry (Fig. 6). All three of the models produce similar strike-slip rates for the Garnet Hill strand and the northern portions of the Banning and Mission Creek strands. The models show some differences in strike-slip rate near Biskra Palms, where the Coachella Valley segment of the San Andreas fault branches to the vertical Mission Creek and north-dipping Banning strands. There, Model D produces greater strike-slip rate (~1 mm/yr) on the Banning strand relative to the other two models. These differences are due to the different transitions from the vertical or dipping Coachella segment of the San Andreas fault to the other fault strands in each model. All three models produce modest right-lateral strike-slip rates (<2.2 mm/yr) on secondary faults in the Indio Hills and Mecca Hills regions, with Model H producing the greatest strike-slip rates on these faults. Model D produces slight (up to 0.5 mm/yr) left-lateral strike-slip rates on some sections of these secondary faults.

Both Models D and H produce slightly lower strike-slip rates on portions of the Coachella Valley segment relative to Model V. Model H produces a strike-slip rate ~1 mm/yr lower for the section of the Coachella segment adjacent to the Hidden fault (Fig. 6, between 50 and 95 km on *x*-axis), and it produces a slightly greater strike-slip rate (<0.5 mm/yr) on the southernmost part of the strand, south of the Hidden fault. Model D produces strike-slip rates up to ~1.5 mm/yr lower than Model V on the Coachella strand in the Mecca Hills region. These differences are modest compared to the total strike-slip rate accommodated on the fault, suggesting that the dip of the fault, and the presence of the Hidden fault and secondary faults, do not substantially alter the fault's ability to accommodate strike slip.

### Comparison of Strike-Slip Rates with Geologic Rates

To date, strike-slip rates have been measured at three sites along the San Andreas fault in the Coachella Valley: excavated exposures at Biskra Palms (Behr et al., 2010) and offset channels near Thousand Palms Oasis (Fumal et al., 2002) and Pushawalla Canyon (Blisniuk et al., 2012). All of our model results fall within the geologic slip rate at Biskra Palms of 12–22 mm/yr, with a preferred rate of 14–17 mm/yr. A new rate from Blisniuk et al. (2012) of 17–24 mm/yr on the Mission Creek strand is much higher than these model results. Previous geologic studies in this region of complex faulting have not found evidence for Holocene offset on the Mission Creek strand farther to the north (Yule and Sieh, 2003), and thus this strand has been mapped in the U.S. Geological Survey (USGS) Quaternary Fault

TABLE 1. WEIGHTED AVERAGE DIP-SLIP RATES

| Fault | SAF > SJF Dip slip (mm/yr) | SAF = SJF Dip slip (mm/yr) |
|---|---|---|
| San Jacinto fault (SJF) | | |
| San Jacinto Valley | 0.26 ± 0.03 | 0.31 ± 0.03 |
| Anza/Clark | –0.47 ± 0.03 | –0.47 ± 0.03 |
| Coyote Creek | –0.14 ± 0.02 | –0.11 ± 0.03 |
| San Andreas fault (SAF) | | |
| San Bernardino | –2.06 ± 0.11 | –2.02 ± 0.11 |
| San Gorgonio Pass | –2.41 ± 0.15 | –2.24 ± 0.15 |
| Banning | –0.49 ± 0.11 | –0.56 ± 0.10 |
| Garnet Hill | –1.66 ± 0.13 | –1.58 ± 0.12 |
| Mission Creek | 0.10 ± 0.13 | 0.11 ± 0.12 |
| Coachella Valley | –0.64 ± 0.06 | –0.47 ± 0.06 |
| Secondary faults in Mecca Hills | | |
| Painted Canyon | 1.30 ± 0.11 | 1.36 ± 0.11 |
| Platform | 0.28 ± 0.05 | 0.31 ± 0.06 |
| Hidden Springs | –0.43 ± 0.05 | –0.44 ± 0.05 |

*Note:* Weighted average dip-slip rates (negative values are reverse slip or east-side up for vertical faults) with standard deviation of spatial variability for models with equal (SAF = SJF)* and unequal (SAF > SJF)* partitioning of slip at the southern boundary of model.

*SAF = SJF denotes 17.55 mm/yr of slip on each fault at the model boundary. SAF > SJF denotes 25 mm/yr on the SAF and 10 mm/yr on the SJF at the model boundary.

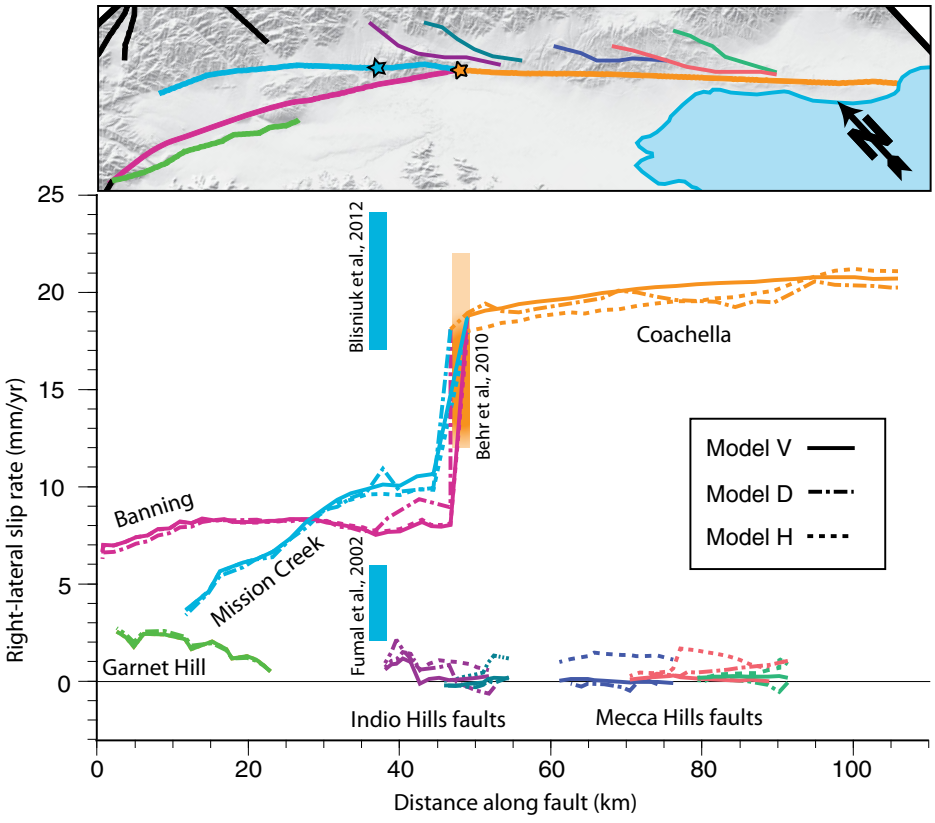


**Figure 6. Right-lateral strike-slip rates along the surface trace of the San Andreas fault system and nearby faults, averaged from models with tectonic loading at fastest and slowest rates. Rates obtained from geologic studies shown as vertical bars. New rates from Blisniuk et al. (2012) are well outside of the rates obtained from modeling and highlight the need for further geologic constraints on slip rates in the region.**

Database as inactive northwest of Highway 62 (Fig. 1; USGS, 2013). The termination of fault activity to the north should limit strike-slip rates on the Mission Creek strand, as seen in the model results (Fig. 6). The higher rate from Blisniuk et al. (2012) on the Mission Creek strand indicates that active faulting in this region may be more complex than currently interpreted, and further study is required to resolve these discrepancies. Strike-slip rates along faults in the Mecca Hills are not well known. The Painted Canyon fault has documented right-lateral offset, and other faults in the area show evidence for right-lateral slip (Sheridan and Weldon, 1994). For the region of this study, the geologically observed strike-slip rates cannot be used to distinguish between alternative configurations of the San Andreas fault because the differences in strike-slip rate between the three alternative models presented here are much smaller than the published ranges for geologically observed slip rates (Fig. 6).

### Coachella Valley Uplift

The three alternative San Andreas fault structural models do not produce large differences in strike-slip rate distribution, but they do produce distinctive dip-slip rates and uplift patterns (Fig. 7). We adjust the surface uplift rates produced by the models to account for isostasy using a crustal flexure model of an elastic crust over a viscous mantle. Following Cooke and Dair (2011), we use a mantle density of 4100 kg/m$^3$, crustal density of 2700 kg/m$^3$, and a flexural rigidity of the crust of $2 \times 10^{23}$ Pa·m$^3$ for our correction.

Model V and Model H both produce relatively uniform and moderate uplift between the San Andreas and San Jacinto faults, contrary to observed tilting with uplift in the Santa Rosa Mountains and relative subsidence in the Coachella Valley southwest of the San Andreas fault (Langenheim et al., 2005; Dorsey et al., 2012). All of the models produce uplift on the northeast side of the Clark fault segment of the San Jacinto fault, where rapid uplift is observed in the Santa Rosa Mountains (location 1, Fig. 7) (Matti et al., 2002). Uplift on the northeast side of the San Jacinto fault is enhanced in Model D relative to the other models. Model D also produces a gradient of uplift that decreases from southwest to northeast between the San Jacinto and San Andreas faults, with moderate subsidence on the SW side of the San Andreas fault (location 2, Fig. 7). The uplift pattern in Model D, which has a single active fault surface that dips to the northeast, best matches the tilting of the Coachella Valley interpreted from increasing sediment thickness from west to east across the Coachella Valley (Langenheim et al., 2005).

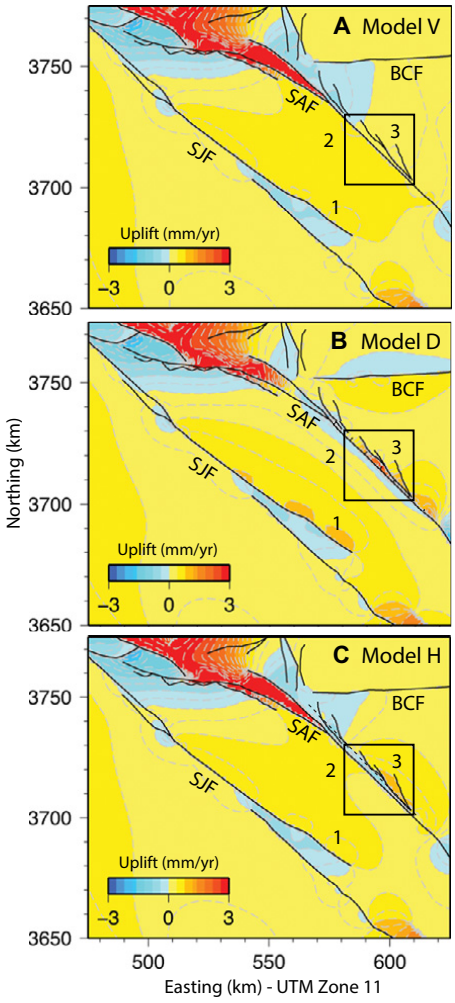


**Figure 7. Contoured uplift rates in the Coachella Valley region, corrected for isostasy. (A) Model V produces relatively uniform uplift between the San Andreas fault (SAF) and San Jacinto fault (SJF) (1 and 2), as well as drop-down on the NE side of the SAF in the Mecca Hills region (3). (B) Model D matches the tilting pattern geologically observed between the SJF and SAF by producing enhanced uplift on the NE side of the Clark fault segment of the SJF (1) and decreasing uplift eastward across the valley (2). Model D also produces localized uplift on the NE side of the SAF in the Mecca Hills region (3). (C) Model H produces the similar uniform uplift between the SAF and SJF as Model V (1 and 2), and enhanced subsidence on the NE side of the SAF (3). Dashed line indicates position of "Hidden" fault at depth. Boxes outline Mecca Hills region explored in Figure 9. SAF—San Andreas fault; SJF—San Jacinto fault; BCF—Blue Cut fault.**

In the Mecca Hills, exposure of the Late Pliocene–Early Pleistocene Mecca Conglomerate west of the Painted Canyon fault implies fast, recent uplift rates in this region (Sylvester and Smith, 1976; McNabb, 2013; McNabb et al., 2013). In contrast to this observation, Model V produces relative uplift southwest of the San Andreas fault in the southern Coachella Valley and fails to produce the uplift observed between the Painted Canyon fault and San Andreas fault (location 1, Fig. 8). Model H produces subsidence between the Painted Canyon fault and San Andreas fault rather than the observed uplift. The only model that matches the observed uplift between the Painted Canyon fault and San Andreas fault is Model D, which has very rapid (2.3 mm/yr) uplift in this area. Model D also matches the northeast-side-down sense of motion observed on the Platform fault (Sylvester and Smith, 1976; Sheridan and Weldon, 1994; location 2, Fig. 8). Of the three alternative fault configurations for the Coachella Valley segment of the San Andreas fault, Model D with a single northeast-dipping fault surface best matches the general uplift pattern observed in the Mecca Hills.

Just to the southeast of the Mecca Hills, Durmid Hill (see Fig. 1 for location) is a region with well-documented uplift between 3 and 4 mm/yr (Bilham and Williams, 1985; Sylvester et al., 1993). While none of the models produce uplift rates as high as 3–4 mm/yr, Model D produces the highest rate of uplift in this region (1.24 mm/yr). Model H produces a much smaller rate of uplift (0.38 mm/yr), and Model V does not produce appreciable uplift. Again, Model D best matches the documented pattern of uplift.

Model D produces a notably different uplift pattern than Model V or H northeast of the Mission Creek fault and around the Blue Cut fault (Fig. 7). Dip slip on the Blue Cut fault is enhanced in Model D, producing moderate subsidence north of the fault and uplift south of the fault. In a geodetic study of the region, Spinler et al. (2010) modeled slip rates on the Blue Cut fault, but the study is inconclusive about the

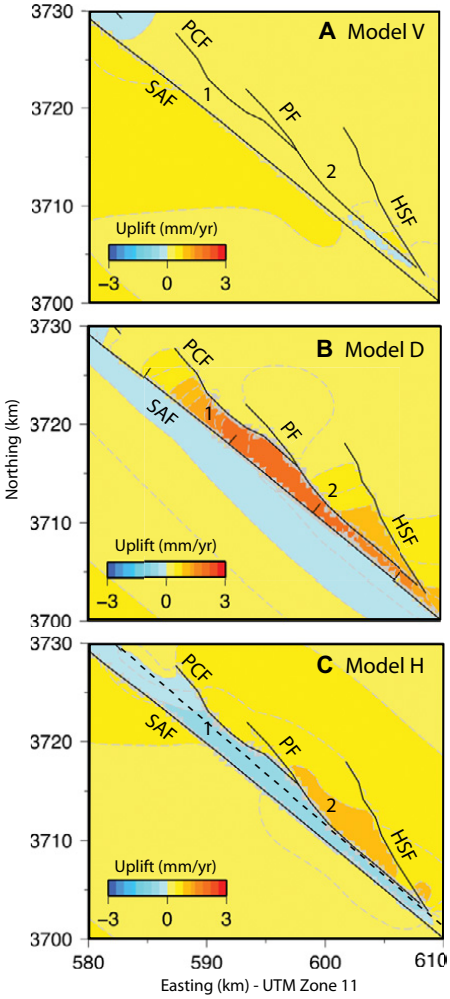


**Figure 8. Contoured uplift rates in the Mecca Hills region corrected for isostasy. (A) Model V does not produce uplift SW of the Painted Canyon fault (PCF). (B) Model D produces significant localized uplift in the Mecca Hills on the SW side of the PCF, matching the geologically observed uplift pattern in the region. (C) Model H produces subsidence between the PCF and San Andreas fault (SAF), contrary to geologic observations. Dashed line indicates position of "Hidden" fault at depth. SAF—San Andreas fault; PCF—Painted Canyon fault; PF—Platform fault; HSF—Hidden Springs fault.**

magnitude and orientation of dip slip on the Blue Cut fault.

Just to the southwest, another area where uplift in Model D differs from Models V and H is between the Banning and Mission Creek strands of the San Andreas fault, near their intersection with the Coachella Valley segment of the San Andreas fault. Models V and H both produce rapid uplift (>3 mm/yr), whereas Model D produces minor subsidence. At present, uplift rates in this region are not well understood, and further data would be needed to distinguish if any of the models are accurately simulating the vertical deformation here. All models reproduce the uplift observed in the San Bernardino Mountains.

## DISCUSSION

Our models of the Coachella Valley in southern California demonstrate the sensitivity of uplift pattern to changes in fault geometry. Outstanding questions relate to (1) why a model with a San Andreas fault that dips produces uplift, while a model with a vertical San Andreas fault does not; (2) the degree of error that vertical San Andreas fault models may incur when simulating regional deformation; and (3) the effect of a dipping San Andreas fault on regional seismic hazard.

### Why Uplift of the Mecca Hills Region?

The geologic observations and model results both show significant recent uplift in the Mecca Hills. The source of this localized uplift in the model with a dipping San Andreas fault is regional transpression along this part of the plate boundary. The Coachella Valley segment of the San Andreas fault has an average strike of 315°, which deviates 5° to 10° from the regional plate velocities (320°–325°; DeMets et al., 2010). This tectonic loading produces transpression on this section of the fault with 9%–18% of the loading partitioned as local contraction rather than 100% strike slip. The maximum rate of model uplift in the Mecca Hills is ~2.3 mm/yr, and strike-slip rates in the region average ~20 mm/yr. Since $\tan^{-1}(2.3/20) = 6.6°$, this ratio of uplift to strike-slip rate is consistent with the expected ratio of contraction to strike-slip resulting from 5° to 10° of transpressional tectonic loading on this section of the San Andreas fault. Not all of the regional compression will be directly expressed as uplift because various deformation mechanisms may occur in the rocks around the faults. The obliquity of the tectonic loading induces transpression along both vertical and dipping faults; the difference lies in how the models express the compressional component of loading. Model D produces uplift expected in the Mecca Hills, whereas Models V and H do not. In Model D, the dip of the Coachella Valley segment allows for the fault-perpendicular compression to be accommodated by reverse slip on the fault. By contrast, in Model V, compression across the vertical Coachella Valley segment of the San Andreas fault increases the normal compression across this fault but does not result in reverse slip. Model H displays a combination of these mechanisms for accommodating compression, with small amounts of reverse slip on the blind and dipping Hidden fault as well as somewhat higher compressive stresses across the Coachella Valley segment of the San Andreas fault. Consequently, the uplift patterns in Models V and H show broad regions of general uplift rather than localized uplift within the Mecca Hills (Fig. 7).

To rule out other sources for the localized uplift at Mecca Hills in the models, we apply tectonic loading parallel to the Coachella Valley segment in Model D to eliminate the compressional loading on this segment (Fig. 9). This slight change in orientation of loading has a major impact on the distribution of uplift and subsidence. Most significantly, the sense of dip slip on the Coachella Valley segment of the San Andreas fault changes. The model simulating realistic plate motion (320°) produces reverse slip on the San Andreas fault and subsequent uplift northeast of the fault. By contrast, when loading is applied parallel to the San Andreas fault (314°), the San Andreas fault experiences normal slip and subsidence northeast of the fault. Consequently, the model without transpression on the San Andreas fault does not produce the localized uplift in the Mecca Hills. The change in dip-slip sense on the San Andreas fault also eliminates the subsidence observed southwest of the San Andreas fault. This change, in combination with decreased uplift northeast of the San Jacinto fault in the Santa Rosa Mountains in this model, reduces the northeast tilting between the San Andreas and San Jacinto faults that we observe in Model D under realistic plate velocity orientations. These results demonstrate that transpression caused by the small degree of obliquity of plate motion relative to the San Andreas fault is the driving factor that produces the distinctive uplift patterns observed around the Coachella Valley.

These results also show that the expression of transpression strongly depends on fault geometry. Transpression across vertical faults may be expressed as distributed deformation rather than localized reverse slip and associated uplift. Furthermore, a small degree of obliquity (<20%) can result in significant localized uplift rates of 2.3 mm/yr. The reverse slip rates are smaller than the strike-slip rates, but the accumulated uplift facilitated by secondary faults produces a distinct uplift pattern.

Fault connectivity also influences the degree of reverse slip along the secondary faults. The secondary faults within the Indio and Mecca Hills in the SCEC CFM v. 4.0 connect at depth with the northeast-dipping Hidden fault. In

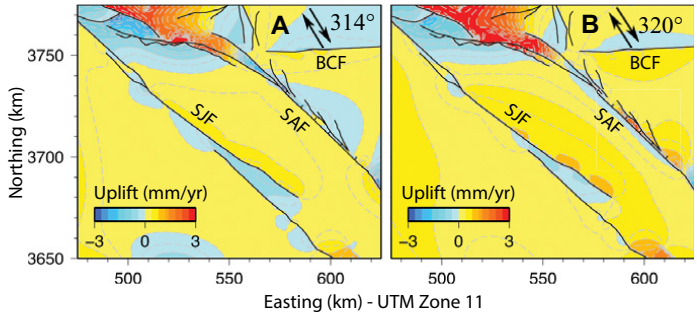


**Figure 9. Contoured uplift rates in the Coachella Valley region for preferred Model D, corrected for isostasy. (A) Uplift rates obtained from tectonic loading applied at 314°, subparallel to the average trace of the Coachella Valley segment of the San Andreas fault (SAF) and (B) tectonic loading applied at 320°, true to observation of relative plate motion between Pacific and North American plates.**

Model D, they merge at depth with the dipping San Andreas fault; however, the secondary faults do not intersect with the vertical San Andreas fault in Model V. Because of this reduced connectivity, we are not surprised that Model V produces very little dip slip and associated localized uplift on these faults relative to Models D and H.

It is worthy of note that the uplift patterns within the Mecca Hills have changed over time, with evidence for both contractional and extensional features in the area. For example, the Painted Canyon fault experiences compression today, but stratigraphy indicates that it was previously an extensional feature. Questions remain as to the mechanisms by which fault structures in the Mecca Hills have formed, shut down, and reactivated throughout evolving transtensional and transpressional regimes and the mechanisms by which the stresses in the area have changed over time. Future mechanical models should explore the evolution of the fault system in this area and may shed light onto the mechanisms that localized faulting, folding, and uplift in the Mecca Hills.

### How Wrong Is the Deformation in Models that Currently Use a Vertical Coachella Segment?

Our model results suggest that models using a vertical Coachella Valley segment may produce a reasonable match to strike-slip rates in the region but will underestimate reverse slip and consequent vertical deformation. Simulations of vertical deformation and ground shaking will be substantially affected by the difference between vertical and dipping fault geometry.

Models that use geodetic data to constrain fault activity produce slip rates for this segment of the San Andreas fault in the range of 16.7 to 25 mm/yr (Becker et al., 2005; Fay and Humphreys, 2005; Meade and Hager, 2005; Fialko, 2006; Lundgren et al., 2009; Spinler et al., 2010). These models all implement a vertical San Andreas fault, and the slip rates overlap the geologically constrained rate at Biskra Palms of 12–22 mm/yr. In a recent study exploring the impact of the dip of the San Andreas fault, Lindsey and Fialko (2013) saw that a northeast-dipping San Andreas fault produces a best fit to InSAR data with slower strike-slip rate on the Coachella Valley segment of the San Andreas fault compared to the vertical San Andreas fault (19 versus 25 mm/yr). Because the Lindsey and Fialko (2013) analysis uses line of sight from InSAR in addition to GPS, the comparison includes a vertical component of deformation, which is an expression of the local compression. As a result, Lindsey and Fialko (2013) find that the dipping San Andreas fault produces a better match to the InSAR data than the vertical alternative. These results confirm our analysis that inclusion of vertical motion gives a more complete understanding of fault slip rates and deformation along the San Andreas fault system. Although models with the vertical San Andreas fault can produce reasonable strike-slip rates, these models will miss a significant portion of the deformation.

## HOW DOES FAULT GEOMETRY AFFECT SEISMIC HAZARD?

A dipping Coachella segment of the San Andreas fault has greater surface area within the seismogenic crust than a vertical San Andreas fault, enhancing the magnitude of potential earthquakes along this segment of the fault. The "Shakeout scenario" simulated a rupture on this section of the fault down to 11.1 km, from Biskra Palms to Bombay Beach, a 69.22 km trace length (Jones et al., 2008). The change from a vertical fault to one that dips 65° yields a 10.3% increase in the surface area of the fault, yielding a proportionate increase in the seismic moment (Spence et al., 1989). In addition, strike-slip rupture along dipping fault surfaces produces different ground shaking than strike-slip rupture along vertical faults (e.g., Oglesby et al., 2000; Fuis et al., 2013). For example, Fuis et al. (2013) simulated a probable rupture on a dipping Coachella Valley segment of the San Andreas fault and found that ground shaking increased by as much as a factor of 2 in the hanging wall, and decreased by the same amount in the footwall. This result means that earthquake hazard for population centers in the Coachella Valley may be lower than previous assessments would suggest. To date, large-scale efforts to characterize seismic hazard in southern California have assumed vertical fault geometry for the Coachella Valley segment of the San Andreas fault (Jones et al., 2008; Working Group on California Earthquake Probabilities, 2008) and thus may be misrepresenting the hazard posed by rupture on this section of the fault.

## CONCLUSIONS

We simulate deformation on alternative fault configurations for the Coachella Valley segment of the San Andreas fault. Varying the dip of the fault in three-dimensional mechanical models does not produce significantly different distributions of strike-slip rates that could give preference to one model over another based on currently available geologic rates. However, the alternative fault configurations produce significant variability in uplift patterns. Model D, which includes a northeast-dipping Coachella Valley segment, produces a substantially better match to patterns of uplift, subsidence, and tilting between the San Andreas and San Jacinto faults, and localized uplift in the Mecca Hills. The models of the southern San Andreas fault demonstrate that a Coachella Valley segment with a 60°–70° NE dip is a mechanically viable geometric interpretation of the active fault surface. The fault structures in Model D agree with distributions of local seismicity, and they are consistent with geodetic observations of recent strain. Crustal deformation models that neglect the northeast dip of the San Andreas fault in the Coachella Valley will not replicate the ground shaking in the region and therefore inaccurately estimate seismic hazard.

#### ACKNOWLEDGMENTS

Many key geologic observations used in the assessment of our models are from recent research by R.J. Dorsey and V.E. Langenheim. This work was funded by National Science Foundation (NSF) grants NSF-

EAR-1145067 to Cooke and EAR-1144946 to Dorsey. Thanks to George Hilley for providing a MATLAB script for isostatic adjustment of uplift rates. The authors thank James McNabb and Bernard Housen for valuable feedback and discussions in the field and Justin Herbert, Elizabeth Madden, and William Clements for their helpful feedback on figures and manuscripts. We also thank an anonymous reviewer for valuable feedback that improved the accuracy and clarity of the manuscript.

**REFERENCES CITED**

Axen, G.J., and Fletcher, J.M., 1998, Late Miocene–Pleistocene extensional faulting, northern Gulf of California, Mexico and Salton Trough, California: International Geology Review, v. 40, p. 217–244, doi:10.1080/00206819809465207.

Bauer, K., Ryberg, T., Fuis, G.S., Goldman, M.R., Catchings, R.D., Rymer, M.J., Hole, J.A., and Stock, J.M., 2013, Investigating the San Andreas fault system in the northern Salton Trough by a combination of seismic tomography and pre-stack depth migration: Results from the Salton Seismic Imaging Project (SSIP): San Francisco, California, American Geophysical Union Fall Meeting, Abstract T14C-05.

Becker, T.W., Hardebeck, J.L., and Anderson, G., 2005, Constraints on fault slip rates of the southern California plate boundary from GPS velocity and stress inversions: Geophysical Journal International, v. 160, p. 634–650, doi:10.1111/j.1365-246X.2004.02528.x.

Behr, W.M., Rood, D.H., Fletcher, K.E., Guzman, N., Finkel, R., Hanks, T.C., Hudnut, K.W., Kendrick, K.J., Platt, J.P., Sharp, W.D., Weldon, R.J., and Yule, J.D., 2010, Uncertainties in slip-rate estimates for the Mission Creek strand of the southern San Andreas fault at Biskra Palms Oasis, southern California: Geological Society of America Bulletin, v. 122, p. 1360–1377, doi:10.1130/B30020.1.

Bilham, R., and Williams, P., 1985, Sawtooth segmentation and deformation processes on the southern San Andreas fault, California: Geophysical Research Letters, v. 12, p. 557–560, doi:10.1029/GL012i009p00557.

Blisniuk, K., Oskin, M., Sharp, W., Rockwell, T., and Fletcher, K., 2011, Slip rates on the southern San Jacinto fault and Holocene–late Pleistocene kinematics of the Pacific-North American plate boundary (abstracts with programs): Southern California Earthquake Center Annual Meeting A-152, September 11–14.

Blisniuk, K., Scharer, K.M., Sharp, W.D., Burgmann, R., Rymer, M.J., Rockwell, T.K., and Williams, P.L., 2012, Rapid late Quaternary slip on the San Andreas fault zone in the Coachella Valley and the distribution of slip across the Pacific–North America plate boundary: San Francisco, California, American Geophysical Union, Abstract G22B-05 presented at 2012 Fall Meeting, 3–7 December.

Boley, J.L., Stimac, J.P., Weldon, R.J., and Rymer, M.J., 1994, Stratigraphy and paleomagnetism of the Mecca and Indio Hills, Southern California: Geological Society of America, Cordilleran Section, Annual Meeting, Guidebook. 27, p. 336–344.

Carena, S., Suppe, J., and Kao, H., 2004, Lack of continuity of the San Andreas Fault in Southern California: Three-dimensional fault models and earthquake scenarios: Journal of Geophysical Research: Solid Earth, v. 109, no. B4, doi:10.1029/2003JB002643.

Cooke, M.L., and Dair, L.C., 2011, Simulating the recent evolution of the southern big bend of the San Andreas fault, southern California: Journal of Geophysical Research, v. 116, p. B04405, doi:10.1029/2010JB007835.

Crouch, S.L., and Starfield, A., 1990, Boundary Element Methods in Solid Mechanics: London, Unwin Hyman Press.

Dair, L., and Cooke, M.L., 2009, San Andreas fault geometry through the San Gorgonio Pass, California: Geology, v. 37, no. 2, p. 119–122, doi:10.1130/G25101A.1.

DeMets, C., Gordon, R.G., and Argus, D.F., 2010, Geologically current plate motions: Geophysical Journal International, v. 181, no. 1, p. 1–80, doi:10.1111/j.1365-246X.2009.04491.x.

Dibblee, T.W., Jr., 1986, Geology of the Imperial Valley region, California, *in* Guptil, P.D., Gath, E.M., and Ruff, R.W., eds., Geology of the Imperial Valley, California: South Coast Geological Society, Santa Ana, California, Annual Symposium and Guidebook, no. 14, p. 1–14.

Dibblee, T.W., Jr., 1997, Geology of the southeastern San Andreas fault zone in the Coachella Valley area, Southern California, *in* Baldwin, J., Lewis, L., Payne, M., and Rocquemore, G., eds., Southern San Andreas fault, Whitewater to Bombay Beach, Salton trough, California: South Coast Geological Society, Annual Field Trip Guide Book, no. 25, p. 35–56.

Dorsey, R.J., Langenheim, V.E., and McNabb, J.C., 2012, Geometry, timing, and rates of active northeast tilting across the southern Coachella Valley and Santa Rosa Mountains: San Francisco, California, American Geophysical Union Abstract T51B-2568, presented at the 2012 Fall Meeting.

Fay, N., and Humphreys, G., 2005, Fault slip rates, effects of elastic heterogeneity on geodetic data, and the strength of the lower crust in the Salton Trough region, southern California: Journal of Geophysical Research: Solid Earth, v. 110, p. B09401, doi:10.1029/2004JB003548.

Fialko, Y., 2006, Interseismic strain accumulation and the earthquake potential on the southern San Andreas fault system: Nature, v. 441, p. 968–971, doi:10.1038/nature04797.

Fuis, G.S., Scheirer, D.S., Langenheim, V.E., and Kohler, M.D., 2012, A new perspective on the geometry of the San Andreas fault in southern California and its relationship to lithospheric structure: Bulletin of the Seismological Society of America, v. 102, p. 236–251, doi:10.1785/0120110041.

Fuis, G.S., Bauer, K., Graves, R.W., Aagaard, B.T., Catchings, R.D., Goldman, M.R., Hole, J.A., Langenheim, V.E., Ryberg, T., Rymer, M.J., Scheirer, D.S., and Stock, J.M., 2013, Geometry of the San Andreas fault in the Salton Trough and its effect on simulated shaking for a rupture similar to that of the Great California Shakeout of 2008: San Francisco, California, American Geophysical Union Abstract T11D-2477 presented at 2013 Fall Meeting, 9–13 December.

Fumal, T.E., Rymer, M.J., and Seitz, G.G., 2002, Timing of large earthquakes since A.D. 800 on the Mission Creek strand of the San Andreas fault zone at Thousand Palms Oasis, near Palm Springs, California: Bulletin of the Seismological Society of America, v. 92, no. 7, p. 2841–2860, doi:10.1785/0120000609.

Griffith, W.A., and Cooke, M.L., 2004, Mechanical validation of the three-dimensional intersection geometry between the Puente Hills blind-thrust system and the Whittier fault, Los Angeles, California: Bulletin of the Seismological Society of America, v. 94, p. 493–505, doi:10.1785/0120030094.

Herbert, J.W., and Cooke, M.L., 2012, Sensitivity of the southern San Andreas fault system to tectonic boundary conditions and fault configurations: Bulletin of the Seismological Society of America, v. 102, p. 2046–2062, doi:10.1785/0120110316.

Herbert, J.W., Cooke, M.L., Oskin, M., and Difo, O., 2014, How much can off-fault deformation contribute to the slip rate discrepancy within the eastern California shear zone?: Geology, v. 42, no. 1, p. 71–75, doi:10.1130/G34738.1.

Janecke, S.U., Dorsey, R.J., Forand, D., Steely, A.N., Kirby, S.M., Lutz, A.T., Housen, B.A., Belgarde, B., Langenheim, V.E., and Rittenour, T.M., 2010, High Geologic Slip Rates since Early Pleistocene Initiation of the San Jacinto and San Felipe Fault Zone in the San Andreas Fault System: Southern California, USA: Geological Society of America Special Paper 475, p. 1–48, doi:10.1130/2010.2475.

Jennings, C.W., compiler, 1977, Geologic map of California: California Division of Mines and Geology Geologic Data Map 2, scale 1:750,000.

Jones, L.M., Bernknopf, R., Cox, D., Goltz, J., Hudnut, K., Mileti, D., Perry, S., Ponti, D., Porter, K., Reichle, M., Seligson, H., Shoaf, K., Treiman, J., and Wein, A., 2008, The ShakeOut Scenario: U.S. Geological Survey Open-File Report 2008-1150 and California Geological Survey Preliminary Report 25 [http://pubs.usgs.gov/of/2008/1150/].

Keller, E.A., Bonkowski, M.S., Korsch, R.J., and Shlemon, R.J., 1982, Tectonic geomorphology of the San Andreas fault zone in the southern Indio Hills, Coachella Valley, California: Geological Society of America Bulletin, v. 93, p. 46–56, doi:10.1130/0016-7606(1982)93<46:TGOTSA>2.0.CO;2.

Kendrick, K.J., Morton, D.M., Wells, S.G., and Simpson, R.W., 2002, Spatial and temporal deformation along the northern San Jacinto fault, southern California: Implications for slip rates: Bulletin of the Seismological Society of America, v. 92, no. 7, p. 2782–2802, doi:10.1785/0120000615.

Langenheim, V.E., Jachens, R.C., Matti, J.C., Hauksson, E., Morton, D.M., and Christensen, A., 2005, Geophysical evidence for wedging in the San Gorgonio Pass structural knot, southern San Andreas fault zone, southern California: Geological Society of America Bulletin, v. 117, p. 1554, doi:10.1130/B25760.1.

Langenheim, V.E., Biehler, S., McPhee, D.K., McCabe, C.A., Watt, J.T., Anderson, M.L., Chuchel, B.A., and Stoffer, P., 2007, Preliminary isostatic gravity map of Joshua Tree National Park and vicinity, southern California. U.S. Geological Survey Open-File Report 2007-1218, scale 1:100,000.

Lin, G., 2013, Three-dimensional seismic velocity structure and precise earthquake relocations in the Salton Trough, Southern California: Bulletin of the Seismological Society of America, v. 103, doi:10.1785/0120120286.

Lin, G., Shearer, P.M., and Hauksson, E., 2007, Applying a three-dimensional velocity model, waveform cross correlation, and cluster analysis to locate southern California seismicity from 1981 to 2005: Journal of Geophysical Research, v. 112, p. B12309, doi:10.1029/2007JB004986.

Lindsey, E.O., and Fialko, Y., 2013, Geodetic slip rates in southern San Andreas fault system: Effects of elastic heterogeneity and fault geometry: Journal of Geophysical Research, v. 118, p. 689–697.

Loveless, J.P., and Meade, B.J., 2011, Stress modulation on the San Andreas fault by interseismic fault system interactions: Geology, v. 39, p. 1035–1038, doi:10.1130/G32215.1.

Lundgren, P., Hetland, E.A., Liu, Z., and Fielding, E.J., 2009, Southern San Andreas–San Jacinto fault system slip rates estimated from earthquake cycle models constrained by GPS and interferometric synthetic aperture radar observations: Journal of Geophysical Research, v. 114, B2, p. B02403, doi:10.1029/2008JB005996.

Luo, G., and Liu, M., 2012, Multi-timescale mechanical coupling between the San Jacinto fault and the San Andreas fault, southern California: Lithosphere, v. 4, no. 3, p. 221–229, doi:10.1130/L180.1.

Marshall, S.T., Cooke, M.L., and Owen, S.E., 2008, Effects of nonplanar fault topology and mechanical interaction on fault-slip distributions in the Ventura basin, California: Bulletin of the Seismological Society of America, v. 98, p. 1113–1127, doi:10.1785/0120070159.

Matti, J.C., Morton, D.M., and Cox, B.F., 1992, The San Andreas fault system in the vicinity of the central Transverse Ranges province, Southern California: U.S. Geological Survey Open-File Report 92-354, 49 p.

Matti, J.C., Cox, B., Morton, D.M., Sharp, R.V., and King, T., 2002, Fault-bounded Neogene sedimentary deposits in the Santa Rosa Mountains, southern California: Crustal stretching or transpressional uplift?: Geological Society of America Abstracts with Programs, v. 34, no. 6, p. 124.

McGill, S.F., Owen, L.A., Weldon, R., and Kendrick, K.J., 2012, Latest Pleistocene and Holocene slip rate for the San Bernardino strand of the San Andreas fault, Plunge Creek, southern California: Implications for strain partitioning within the southern San Andreas fault system for the last ~35 k.y.: Geological Society of America Bulletin, v. 125, p. 48–72, doi:10.1130/B30647.1.

McNabb, J.C., 2013, Stratigraphic Record of Pliocene–Pleistocene Basin Evolution and Deformation along the San Andreas fault, Mecca Hills, California [M.S. thesis]: University of Oregon, 70 p.

McNabb, J.C., Dorsey, R.J., Housen, B.A., and Messe, G.T., 2013, Stratigraphic record of basin formation, deformation, and destruction in the past 2 Ma along the southern San Andreas fault, Mecca Hills, Califor-

nia: San Francisco, California, American Geophysical Union Abstract T11D-2484, presented at Fall Meeting.

Meade, B.J., and Hager, B.H., 2005, Block models of crustal motion in southern California constrained by GPS measurements: Journal of Geophysical Research, v. 110, p. B03403, doi:10.1029/2004JB003209.

Meigs, A.J., Cooke, M.L., and Marshall, S.T., 2008, Using vertical rock uplift patterns to constrain the three-dimensional fault configuration in the Los Angeles Basin: Bulletin of the Seismological Society of America, v. 98, p. 106–123, doi:10.1785/0120060254.

Messe, G.T., McNabb, J.C., Housen, B.A., and Dorsey, R.J., 2012, Magnetostratigraphy of the Palm Spring Formation, Mecca Hills, California: Geological Society of America Abstracts with Programs, v. 44, no. 7, p. 76.

Messe, G.T., Housen, B.A., Burmester, R.F., McNabb, J.C., and Dorsey, R.J., 2013, Magnetostratigraphy and Paleocurrent Directions for the Upper Member of the Palm Spring Formation, Mecca Hills, California: San Francisco, California, American Geophysical Union Abstract GP41A-1108, presented at the 2013 Fall Meeting.

Nicholson, C., Plesch, A., Shaw, J., and Hauksson, E., 2012, Upgrades and Improvements to the SCEC Community Fault Model: Increasing 3D fault complexity and compliance with surface and subsurface data (abstracts with programs): Southern California Earthquake Center Annual Meeting 122, September 8–12.

Nicholson, C., Plesch, A., Shaw, J., Sorlein, C., and Hauksson, E., 2013, Updating the 3D fault set for the SCEC Community Fault Model (CFM-v4) and revising its associated fault database (abstracts with programs): Southern California Earthquake Center Annual Meeting 123, September 8–11.

Oglesby, D.D., Archuleta, R.J., and Nielsen, S.B., 2000, The three-dimensional dynamics of dipping faults: Bulletin of the Seismological Society of America, v. 90, no. 3, p. 616–628, doi:10.1785/0119990113.

Oskin, M., Perg, L., Blumentritt, D., Mukhopadhyay, S., and Iriondo, A., 2007, Slip rate of the Calico fault: Implications for geologic versus geodetic rate discrepancy in the eastern California shear zone: Journal of Geophysical Research, v. 112, no. B03402, p. 1–16, doi:10.1029/2006JB004451.

Philibosian, B.E., Fumal, T., and Weldon, R., 2011, San Andreas Fault earthquake chronology and Lake Cahuilla history at Coachella, California: Bulletin of the Seismological Society of America, v. 101, no. 1, p. 13–38, doi:10.1785/0120100050.

Platt, J.P., and Becker, T.W., 2010, Where is the real transform boundary in California?: Geochemistry Geophysics Geosystems, v. 11, p. Q06012, doi:10.1029/2010GC003060.

Plesch, A., Shaw, J.H., Benson, C., Bryant, W.A., Carena, S., Cooke, M.L., Dolan, J., Fuis, G.S., Gath, E., Grant, L., Hauksson, E., Jordan, T., Kamerling, M., Legg, M., Lindvall, S., Magistrale, H., Nicholson, C., Niemi, N., Oskin, M., Perry, S., Planansky, G., Rockwell, T., Shearer, P., Sorlien, C., Suess, M.P., Suppe, J., Treiman, J., and Yeats, R., 2007, Community fault model (CFM) for Southern California: Bulletin of the Seismological Society of America, v. 97, p. 1793–1802, doi:10.1785/0120050211.

Powell, R.E., 1993, Balanced palinspastic reconstruction of pre-late Cenozoic paleogeology, southern California: Geologic and kinematic constraints on evolution of the San Andreas fault system, *in* Powell, R.E., Weldon, R.J., II, and Matti, J.C., eds., The San Andreas Fault System: Displacement, Palinspastic Reconstruction, and Geologic Evolution: Geological Society of America Memoir 178, p. 1–106, doi:10.1130/MEM178-p1.

Prentice, C.S., Weldon, R.J., and Sieh, K.E., 1986, Distribution of slip between the San Andreas and San Jacinto faults near San Bernardino, southern California: Geological Society of America Abstracts with Programs, v. 18, p. 172.

Rockwell, T.K., 2008, Observations of mode-switching from long paleoseismic records of earthquakes on the San Jacinto and San Andreas faults: Implications for making hazard estimates from short paleoseismic records: Oslo, International Geological Congress, International Union Geol. Sci., Aug. 6–14.

Roeske, S.M., Till, A.B., Foster, D.A., and Sample, J.C., 2007, Introduction, *in* Till, A.B., Roeske, S.M., Sample, J.C., and Foster, D.A., eds., Exhumation Associated with Continental Strike-Slip Fault Systems: Geological Society of America Special Paper 434, p. 7–9.

Rymer, M.J., 1989, New Quaternary age control for strata within the Indio Hills, Southern California: Quarterly of San Bernardino County Museum Association, v. 36, p. 64.

Rymer, M.J., 1991, Geological structure, transpression, and neotectonics of the San Andreas fault in the Salton Trough, California, Part 2: The Bishop ash bed in the Mecca Hills, *in* Wallawender, M.J., and Hannan, B.B., eds., Geological Excursions in Southern California and Mexico: San Diego, California, Geological Society of America Guidebook for the Annual Meeting, p. 388–396.

Rymer, M.J., 1994, Quaternary fault-normal thrusting in the northwestern Mecca Hills, southern California, *in* McGill, S.F., and Ross, T.M., eds., Geological Investigations of an Active Margin: Geological Society of America, Cordilleran Section Guidebook, Trip 15, p. 325–329.

Rymer, M.J., 2000, Triggered surface slips in the Coachella Valley area associated with the 1992 Joshua Tree and Landers, California, earthquakes: Bulletin of the Seismological Society of America, v. 90, p. 832–848, doi:10.1785/0119980130.

Sharp, R.V., 1981, Variable rates of late Quaternary strike-slip on the San Jacinto fault zone, southern California: Journal of Geophysical Research, v. 86, no. B3, p. 1754–1762, doi:10.1029/JB086iB03p01754.

Sheridan, J.M., and Weldon, R.J., II, 1994, Accommodation of compression in the Mecca Hills, California, *in* McGill, S.F., and Ross, T.M., eds., Geological Investigations of an Active Margin: Geological Society of America Guidebook Cordilleran Section; Redlands, California, San Bernardino County Museum, p. 330–336.

Shifflett, H., Gray, M.G., Grannell, R., and Ingram, B.L., 2002, New evidence on the slip rate, renewal time, and late Holocene surface displacement, southernmost San Andreas fault, Mecca Hills, California: Bulletin of the Seismological Society of America, v. 92, p. 2861–2877, doi:10.1785/0120000601.

Sieh, K.E., and Williams, P., 1997, Behavior of the southernmost San Andreas fault during the past 300 years: South Coast Geological Society Annual Field Trip Guidebook, v. 25, p. 332–348.

Smith-Konter, B., and Sandwell, D.T., 2009, Stress evolution of the San Andreas fault system: Recurrence interval versus locking depth: Geophysical Research Letters, v. 36, no. 13, L13304, doi:10.1029/2009GL037235.

Spence, W., Sipkin, S.A., and Choy, G.L., 1989, Measuring the Size of an Earthquake: Earthquakes and Volcanoes, v. 21, no. 1, p. 58–63.

Spinler, J.C., Bennett, R.A., Anderson, M.L., McGill, S.F., Hreinsdóttir, S., and McCallister, A., 2010, Present-day strain accumulation and slip rates associated with southern San Andreas and eastern California shear zone faults: Journal of Geophysical Research, v. 115, p. B11407, doi:10.1029/2010JB007424.

Spotila, J.A., Niemi, N., Brady, R., House, M., Buscher, J., and Oskin, M., 2007, Long-term continental deformation associated with transpressive plate motion: The San Andreas fault: Geology, v. 35, p. 967, doi:10.1130/G23816A.1.

Sylvester, A.G., and Smith, R.R., 1976, Tectonic transpression and basement-controlled deformation in San Andreas fault zone, Salton Trough, California: American Association of Petroleum Geologists Bulletin, v. 60, p. 2081–2102.

Sylvester, A.G., Bilham, R., Jackson, M., and Barrientos, S., 1993, Aseismic growth of Durmid Hill, southeasternmost San Andreas fault, California: Journal of Geophysical Research, v. 98, B8, p. 14,233–14,243, doi:10.1029/93JB01028.

Thomas, A.L., 1993, POLY3D: A three-dimensional, polygonal element, displacement discontinuity boundary element computer program with applications to fractures, faults, and cavities in the Earth's crust [M.S. Dissertation]: Stanford University, Stanford, California, 52 p.

USGS, 2013, Quaternary Faults and Fold Database: http://earthquake.usgs.gov/hazards/qfaults/map/ (accessed December 2013).

van der Woerd, J., Klinger, Y., Sieh, K., Tapponnier, P., Ryerson, F.J., and Mériaux, A.S., 2006, Long-term slip rate of the southern San Andreas fault from $^{10}$Be-$^{26}$Al surface exposure dating of an offset alluvial fan: Journal of Geophysical Research, v. 111, p. B04407, doi:10.1029/2004JB003559.

Weldon, R.J., and Sieh, K.E., 1985, Holocene rate of slip and tentative recurrence interval for large earthquakes on the San Andreas fault, Cajon Pass, southern California: Geological Society of America Bulletin, v. 96, p. 793–812, doi:10.1130/0016-7606(1985)96<793:HROSAT>2.0.CO;2.

Working Group on California Earthquake Probabilities, 2008, The Uniform California Earthquake Rupture Forecast, Version 2 (UCERF 2): U.S. Geological Survey Open-File Report 2007-1437 and California Geological Survey Special Report 203 [http://pubs.usgs.gov/of/2007/1437/].

Yule, D., and Sieh, K., 2003, Complexities of the San Andreas Fault near San Gorgonio Pass; Implications for large earthquakes: Journal of Geophysical Research, v. 108, p. 2548, doi:10.1029/2001JB000451.

Geosphere

# Sensitivity of uplift patterns to dip of the San Andreas fault in the Coachella Valley, California

Laura A. Fattaruso, Michele L. Cooke and Rebecca J. Dorsey

*Geosphere* 2014;10;1235-1246
doi: 10.1130/GES01050.1



**Notes**